The properties and design concepts of photonic directional couplers made of photonic crystal slabs

2010 J. Phys. D: Appl. Phys. 43 465103

(http://iopscience.iop.org/0022-3727/43/46/465103)

IOP PUBLISHING JOURNAL OF PHYSICS D: APPLIED PHYSICS

J. Phys. D: Appl. Phys. **43** (2010) 465103 (7pp) doi:10.1088/0022-3727/43/46/465103

The properties and design concepts of photonic directional couplers made of photonic crystal slabs

Chih-Hsien Huang[1,2], Jing-Nuo Wu[3], Po-Yi Lee[2], Wen-Feng Hsieh[1,2,4] and Szu-Cheng Cheng[3,4]

[1] Institute of Electro-Optical Science and Engineering, National Cheng Kung University, Tainan 701, Taiwan

[2] Department of Photonics and Institute of Electro-Optical Engineering, National Chiao Tung University, Hsinchu 300, Taiwan

[3] Department of Physics, Chinese Culture University, Taipei 111, Taiwan

E-mail: wfhsieh@mail.nctu.edu.tw and sccheng@faculty.pccu.edu.tw

Received 4 June 2010, in final form 30 August 2010
Published 4 November 2010
Online at stacks.iop.org/JPhysD/43/465103

Abstract

The properties and design concepts of air-defect symmetric and asymmetric directional couplers (DCs) made of photonic crystal slabs (PCSs) are investigated by the tight-binding theory. We give criteria in both cases for determining the specific frequency, named as the decoupling point, at which the even (-like) and odd (-like) parities of eigenmodes should switch. Two dispersion curves will cross in symmetric DCs but not in asymmetric DCs because eigenfrequencies of isolated photonic waveguides (PCWs) are different in asymmetric DCs. In the dielectric-rod PCS, the decoupling point of the DC is located almost at the same wave vector as a two-dimensional (2D) DC with only a blue shift in its frequency. Therefore, 2D simulation can give a primary result in designing a dielectric-rod DC. On reducing the radius of the defect rods, the increase in coupling coefficients leads to a faster group velocity and a longer coupling length. On the other hand, the dispersion curves of the air-hole PCS DC are no longer parallel to those of the 2D DC so that performing a 3D simulation is necessary in designing an air-hole PCS DC with enlarged air holes. Moreover, the dispersion curve of the single PCW is no longer located at the centre of the curves of the symmetric DC and the group velocity may become negative which is not observed in the dielectric-rod PCS. The simulation results indicate that the coupling length of an air-defect DC can be achieved as short as 5 lattice constants, which is much smaller than that made of dielectric defects in air-hole PCS DCs.

(Some figures in this article are in colour only in the electronic version)

1. Introduction

A photonic crystal slab (PCS) is a practical structure in which the dielectric media are arranged periodically in two dimensions and a finite size in the other dimension [1, 2]. As a row of dielectric rods or air holes in the PCS is removed or replaced by a new row with a different radius of rods (holes) or other geometric structures [3], the electromagnetic wave will be guided along this line defect or photonic crystal waveguide (PCW) [4–6]. When another waveguide is sculptured in the PCS separated by one or several line(s) of partition rods or holes, an optical coupler can be designed to act as a beam splitter, switch, demultiplexer or filter [7–11].

The PCWs of a directional coupler (DC) are usually made by removing the air holes in the dielectric substrate [7, 9] due to the less scattering loss caused by structural disorder [12] and easy fabrication. However, these PCWs can guide multimode. In order to prevent from operating with multimode propagation, DCs have been designed with three rows of partition holes [13, 14]. As a result, their coupling

[4] Authors to whom any correspondence should be addressed.

lengths are quite long with 20–30a, where a is the lattice constant, and their operation frequencies are limited in the low-frequency region of the photonic band gap. On the other hand, when the PCWs are made by reducing the radius of dielectric rods or enlarging the radius of air holes, i.e. creating air defects, the PCW allows a single-mode propagation and the operation frequency of the DC could cover the entire band gap. Therefore, the air-defect structure seems to be a better choice to design a DC with a short coupling length although it may not tolerate manufacture disorder leading to the scattering loss.

Generally, a three-dimensional (3D) numerical analysis focuses mainly on the single PCW made of PCS with the plane wave expansion method (PWEM) or the finite difference time domain (FDTD) method [3]. Analyses of DCs in the PCS are rare or are focused on a two-dimensional (2D) case in which the height of the slabs are supposed to be infinite [15, 16]. However, in practical applications, the height of the slab should be comparable to the lattice constant of the photonic crystal (PC). Therefore, the effective index method [17, 18] has been used to simplify the simulation of the dielectric-defect PCW made of a PCS into a 2D case, but the effective index obtained from the perfect dielectric slab is not suitable to describe the air-defect PCS because the effective index in the waveguides is smaller than that in the surroundings.

Furthermore, the simulation results obtained from either PWEM or FDTD cannot provide analytic equations to realize the physical properties or to give the design concepts of the DC. The tight-binding theory (TBT) [19, 20], widely used to describe the 2D wave propagating in the coupled resonant optical waveguides [21], has been extended to describe the 2D PCWs made of chains of continuous point defects [22, 23]. Because the electric field is not so localized in PCWs, the extended TBT which considers the coupling beyond the nearest-neighbour point defects should be used [15]. Although we have used this TBT to describe wave propagation in the symmetric and asymmetric DC in a 2D PC made of dielectric rods [16, 22, 24], there are still no reports about the PCS DCs made of both dielectric rods and air holes. Therefore, it is still necessary to derive more general equations to describe the electric field propagation in these practical cases and to give design concepts for these PCS DCs.

In this paper, we first use the TBT to derive the coupled equations to describe the dispersion relation and mode distributions of the symmetric and asymmetric couplers made of a triangular lattice PCS. Second, the physical properties of the PCS DCs are discussed. Third, the 3D simulation done by the PWEM is used to verify our theoretical analyses and to discuss, in more detail, the properties of dielectric-rod and air-hole PCS DCs. Finally, the design concepts of PCS DCs are given by comparing the results obtained with different structures as well as with 2D and 3D simulations.

2. Tight-binding theory

We consider a PCS in which the lattice constant is a. When the radius of a row of dielectric rods (air holes) in a PCS is reduced (enlarged), a PCW is created and it consists of a sequence of identical single-mode defects. As another PCW is carved into this PCS, two PCWs labelled PCW1 and PCW2 are separated by a row of partition rods (holes) to form a DC, as shown in figure 1. The eigenfrequency and the electric field distribution of the isolated point defect in PCW1 are assumed to be ω_1 and $\boldsymbol{E}_1(\boldsymbol{r})$, and those in PCW2 to be ω_2 and $\boldsymbol{E}_2(\boldsymbol{r})$, respectively. The total electric fields in PCW1 and PCW2 can be expressed as the superposition of the point-defect fields. Under the tight-binding approximation, the equations for describing the electric field propagation in the isolated PCW1 and PCW2 are [24]

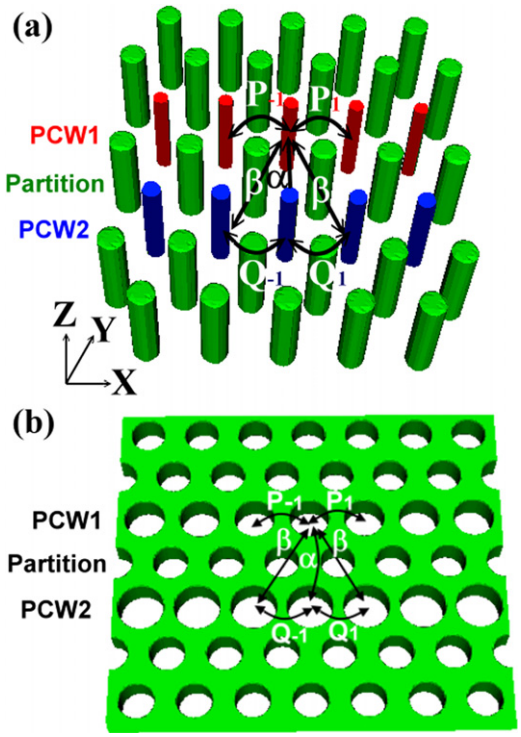

Figure 1. Structures of the couplers made of (a) dielectric rods and (b) air holes. P_i and Q_i are the coupling coefficients within single photonic crystal waveguides (PCW1 and PCW2) separated by a row of partition rods or holes; α and β are the nearest-neighbour and the second nearest-neighbour coupling coefficients between two waveguides.

$$\mathrm{i}\frac{\partial}{\partial t}u_n = (\omega_1 - P_0')u_n - \sum_{m=1}^{3} P_m'(u_{n+m} + u_{n-m}), \qquad (1)$$

$$\mathrm{i}\frac{\partial}{\partial t}v_n = (\omega_2 - Q_0')v_n - \sum_{m=1}^{3} Q_m'(v_{n+m} + v_{n-m}). \qquad (2)$$

Here u_n and v_n are the field amplitudes of site n in these two PCWs; m is an integer; P_m' and Q_m' are the coupling coefficients with the mth nearest-neighbour defects within the isolated PCW1 and PCW2. We consider here only the coupling up to the third nearest-neighbour defect ($m = 3$) in each PCW because the fourth nearest-neighbour coupling coefficient is three orders of magnitude smaller than the nearest-neighbour one. Therefore, the dispersion relations of these PCWs have

the forms

$$\omega_1'(k) = \omega_1 - P_0' - \sum_{m=1}^{3} 2P_m' \cos(mka), \tag{3}$$

$$\omega_2'(k) = \omega_2 - Q_0' - \sum_{m=1}^{3} 2Q_m' \cos(mka), \tag{4}$$

where k is the wave vector of the incident wave. As these two waveguides are arranged close enough, the coupling both within each of the PCWs and between two PCWs must be considered simultaneously. Therefore, the evolution equations for describing the coupled PCWs become

$$\mathrm{i}\frac{\partial}{\partial t}u_n = (\omega_1 - P_0)u_n - \sum_{m=1}^{3} P_m(u_{n+m} + u_{n-m}) - \alpha v_n - \beta(v_{n+1} + v_{n-1}), \tag{5}$$

$$\mathrm{i}\frac{\partial}{\partial t}v_n = (\omega_2 - Q_0)v_n - \sum_{m=1}^{3} Q_m(v_{n+m} + v_{n-m}) - \alpha u_n - \beta(u_{n+1} + u_{n-1}). \tag{6}$$

The coupling coefficient (C_m^{ij}) between the site n of the ith PCW and the site $n+m$ of the jth PCW is defined as

$$C_m^{ij} = \frac{\omega_i \int_{-\infty}^{\infty} \mathrm{d}v \Delta\varepsilon(\boldsymbol{r})\boldsymbol{E}_{in} \cdot \boldsymbol{E}_{jn+m}}{\int_{-\infty}^{\infty} \mathrm{d}v[\mu_0|\boldsymbol{H}_{in}|^2 + \varepsilon|\boldsymbol{E}_{in}|^2]} \tag{7}$$

with $\Delta\varepsilon(\boldsymbol{r}) = \varepsilon'(\boldsymbol{r}) - \varepsilon(\boldsymbol{r})$ being the difference of the perturbed and unperturbed permittivity and C_0^{ii} representing a small shift in frequency arising from the presence of the neighbour defects or cavities. Therefore, P_m or $P_m' = C_m^{11}$, Q_m or $Q_m' = C_m^{22}$, $\alpha = C_0^{12} = C_0^{21}$ and $\beta = C_{\pm1}^{12} = C_{\pm1}^{21}$. $\Delta P_m = P_m - P_m'$ or $\Delta Q_m = Q_m - Q_m'$ is the difference in coupling coefficients within the individual PCW arising from the presence of the other PCW. In general, ΔP_m is approximately equal to 0 in the dielectric-rod PCS; however, $|\Delta P_m|$ may become large in the air-hole PCS due to the less localized electric field in the defects. In other words, the coupling coefficients within the individual PCW will be influenced by the other PCW in the air-hole DC. In addition, in the 2D DC with dielectric rods [24], the eigenfield of the DC is a complete transverse electric wave so that only E_z needs to be taken into consideration and the 2D integral in equation (7) is sufficient. However, in the PCS cases, three components of the electric field should be considered and the integral should also be 3D.

As a monochromatic wave with frequency ω and wave vector k is incident on the DC with $u_m = U_0 \mathrm{e}^{(\mathrm{i}kma - \omega t)}$ and $v_m = V_0 \mathrm{e}^{(\mathrm{i}kma - \omega t)}$, we can substitute these terms into the coupled equations (5) and (6) and obtain these characteristic equations of the DC as [24]

$$(\omega - \bar{\omega}_1)U_0 + g(ka)V_0 = 0, \tag{8}$$

$$(\omega - \bar{\omega}_2)V_0 + g(ka)U_0 = 0. \tag{9}$$

Here $g(ka) = \alpha + 2\beta\cos(ka)$; $\bar{\omega}_1(k)$ and $\bar{\omega}_2(k)$ are as follows:

$$\bar{\omega}_1(k) = \omega_1 - P_0 - \sum_{m=1}^{3} 2P_m \cos(mka), \tag{10}$$

$$\bar{\omega}_2(k) = \omega_2 - Q_0 - \sum_{m=1}^{3} 2Q_m \cos(mka). \tag{11}$$

As $\Delta P_m = \Delta Q_m \approx 0$ is achieved, $\bar{\omega}_1(k)$ and $\bar{\omega}_2(k)$ are reduced to the dispersion relations of PCW1 and PCW2 as $\bar{\omega}_1(k) \approx \omega_1'(k)$ and $\bar{\omega}_2(k) \approx \omega_2'(k)$. In other cases, the dispersions should be modified accordingly. The eigenfrequencies of equations (8) and (9) are

$$\omega^{\pm}(k) = \frac{(\bar{\omega}_1 + \bar{\omega}_2)}{2} \pm \sqrt{\Delta^2 + (g(ka))^2}, \tag{12}$$

where $\Delta = (\bar{\omega}_2 - \bar{\omega}_1)/2$. The amplitude ratios $\chi^{\pm}$ (V_0/U_0) corresponding to frequencies $\omega^{\pm}(k)$ are

$$\chi^{\pm} = (V_0/U_0)^{\pm} = -\frac{\Delta \pm \sqrt{\Delta^2 + (g(ka))^2}}{g(ka)}. \tag{13}$$

In the symmetric DC with identical PCWs, namely $\bar{\omega}_1 = \bar{\omega}_2$, equations (12) and (13) become

$$\omega^{\pm}(k) = \bar{\omega}_1 \mp g(ka) = \bar{\omega}_1 \mp [\alpha + 2\beta\cos(ka)] \tag{14}$$

and $\chi^{\pm} = \pm 1$. We must note that only the optical field with its eigenfrequency on the dispersion curves of equation (12) lying under the light line will be confined in the PCS. We thus, from now on, consider only the PCS DC with confined modes.

3. Dielectric-rod PCS

Observing the eigenmode of the point defect in a triangular lattice in figures 2(*a*)–(*d*), we find that the E_z component of the field is centred and localized within the rod, whereas $E_{\parallel}$ (E_x or E_y) with odd parity is localized in the air. The coupling coefficient contributed by $E_{\parallel}$ is much smaller than that by E_z. Therefore, although $E_{\parallel}$ exists in the eigenmode of the point defect, only E_z needs to be taken into consideration.

Equation (3) describes the dispersion relation of a PCW in which the coupling coefficient $P_1' \approx P_1$ is positive and can be estimated from equation (7). That is, in the air defect $\Delta\varepsilon$ is negative and z component of the electric field $\boldsymbol{E}_1(\boldsymbol{r})$ in the point defect has an opposite sign as it extends to the nearest defect (i.e. $\boldsymbol{E}_{in}\boldsymbol{E}_{in+1} < 0$ or $\boldsymbol{E}_{1z}(\boldsymbol{r})\boldsymbol{E}_{1z}(\boldsymbol{r} - a\boldsymbol{x}) < 0$). Similarly, the second nearest-neighbour coupling coefficient P_2 is negative and generally one order of magnitude smaller than the nearest-neighbour one (P_1) because the electric field around the nearest-neighbour rod is much smaller than that around the second nearest-neighbour rod. When neglecting P_2 for a simple estimation, we can find that the slope of the dispersion curve or the group velocity must be positive or zero.

In the asymmetric coupler, $\bar{\omega}_1 \neq \bar{\omega}_2$ or $\Delta \neq 0$, the dispersion curves will never cross even if $g(ka) = 0$. By varying the magnitude of Δ caused by a difference in the refractive index or radius of the defect rods in each waveguide,

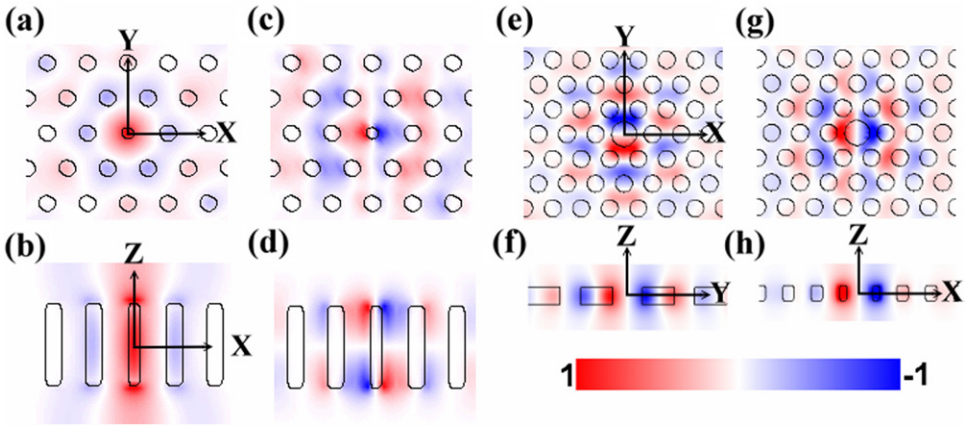

Figure 2. Electric field distribution of E_z for a reduced-rod point defect ($r_d = 0.14a$) in which the radius, dielectric constant and height of the perfect rods are $0.2a$, 12 and $2.0a$ at the planes of (a) $z = 0$ and (b) $y = 0$. Distribution of $E_\parallel$ at the planes of (c) $z = 0.8a$ and (d) $y = 0$. Distribution of E_x for an air-hole point defect ($r_d = 0.44a$) in which the radius of perfect air holes, dielectric constant and height of the slabs are $0.3a$, 12 and $0.55a$ at the planes of (e) $z = 0$ and (f) $x = 0$. Distribution of E_y at the planes of (g) $z = 0$ and (h) $y = 0$.

we can design not only the separation of two dispersion curves but also the mode ratios χ as indicated in equations (12) and (13). When Δ becomes larger, the mode ratio $|\chi|$ departs further from 1, which means the mode parities become more asymmetric. In addition, α and β are both negative because the electric field of the point defect has the same sign as it extends to its nearest and second nearest point defects in the other PCW, namely $\boldsymbol{E}_{1z}(\boldsymbol{r})\boldsymbol{E}_{1z}(\boldsymbol{r} - \sqrt{3}a\boldsymbol{y}) > 0$ and $\boldsymbol{E}_{1z}(\boldsymbol{r})\boldsymbol{E}_{1z}(\boldsymbol{r} - \sqrt{3}a\boldsymbol{y} - a\boldsymbol{x}) > 0$. Therefore, at low k, $g(ka)$ is negative and χ^+ corresponding to the eigenfrequency $\omega^+(k)$ represents the even-like parity of the eigenmode; whereas χ^- corresponding to the eigenfrequency $\omega^-(k)$ represents the odd-like parity of the eigenmode. As k passes the $g(k_d a) = 0$ point, $g(ka)$ becomes positive, and the parties of eigenmodes will switch.

In the symmetric coupler with identical PCWs, when $g(k_d a) = 0$, $\omega^\pm = \bar{\omega}_1$ so that the dispersion curves cross at this point. At this degenerate point, the coupling length of the DC is infinite and the eigenmodes switch. We therefore named this degenerate point as the decoupling point. The criterion for satisfying $g(ka) = 0$ is twice the magnitude of the second nearest-neighbour coupling coefficient ($|\beta|$) must be larger than that of the nearest-neighbour coupling coefficient ($|\alpha|$), i.e. $|2\beta| > |\alpha|$.

Comparing the field distribution (E_z) of a point defect in a PCS at $z = 0$ with that in the 2D case shown in figure 3, we found that the field distributions are similar so that the coupling coefficients should also be similar. However, owing to the fact that the electric field extends outside the slab in the z-direction, the eigenfrequency (ω_1) of the point defect in a PCS should be larger than that in a 2D PC. Therefore, the dispersion curves of the PCWs in these two structures would be almost parallel to each other with only a blue frequency shift for the PCS. The smaller the slab thickness, the larger the blue shift will be. A similar ratio of coupling coefficients β to α makes the crossing point of the couplers almost locate at the same wave vector but with a higher frequency for the PCS case.

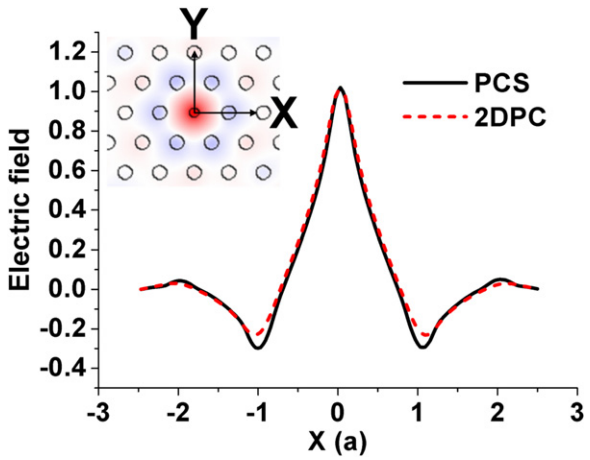

Figure 3. Field distributions of point defects along the x-axis in the 2D PC and the PCS in which the radius and the dielectric constant of the perfect rods are $0.2a$ and 12, and the radius of the reduced rod is $0.14a$. The inset is the electric field distribution of the 2D point defect.

4. Air-hole PCS

The field distributions of the point defects made of an air-hole PCS in figures 2(e)–(h) show that only x and y components of the electric field exist in the eigenmode which will contribute to the coupling coefficients defined in equation (7). The coupling coefficients, P_1' and P_2', of a single PCW are both positive because $\Delta\varepsilon$ is negative for air defect and the electric field has an opposite sign as it extends to the nearest or the second nearest-neighbour defect sites along the x direction. The dispersion relation of a single PCW in equation (3) can be rewritten as $\omega_1'(k) = \omega_1 - P_0' - 2P_1' \cos(ka) - 2P_2' \cos(2ka)$ when P_3' is neglected because of approximately two orders of magnitude smaller than P_1'. Under this circumstance, the slope of the dispersion curve is $2aP_1' \sin(ka) + 4aP_2' \sin(2ka)$ and the dispersion curve may bend downwards as $ka > \pi/2$ or even have a negative group velocity if $|P_2'|$ is sufficiently large. The negative group velocity does not happen at a dielectric-rod PCW in which the sign of P_1' is positive and P_2' is negative.

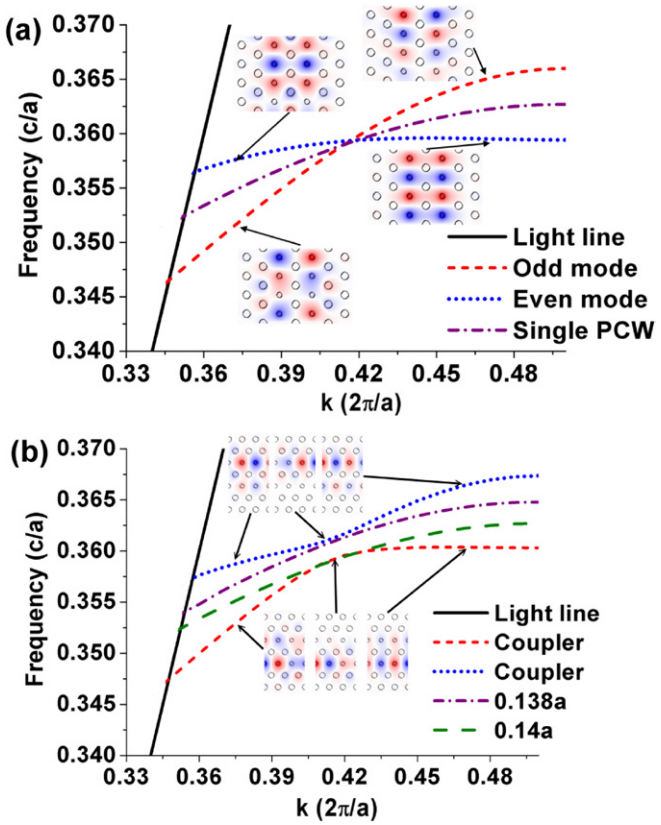

Figure 4. Dispersion relations of the (a) symmetric coupler and (b) asymmetric coupler. The insets are the cross sections of the structures and the eigenmodes of these couplers at $z = 0$.

In the air-hole DCs, because the electric field is not so localized in the defect regions, we obtain $\Delta P_m = P_m - P'_m \neq 0$ and $\omega'_1(k) \neq \bar{\omega}_1(k)$. From the definition of coupling coefficients, one knows ΔP_0 is negative whereas ΔP_1 is positive. At low wave vectors, the dispersion curve of a single PCW locates below the centre of the dispersion curves of a symmetric DC.

5. Simulation results and discussion

In order to verify the prediction made by the TBT, we first consider a symmetric and an asymmetric DC in a triangular lattice in which the radius, height and the dielectric constant of the perfect dielectric rods are $0.2a$, $2.0a$ and 12, respectively. The radius of the dielectric-defect rods in the symmetric DC is $0.14a$ and those in the asymmetric DC are $0.138a$ and $0.14a$, respectively. From the simulation results of the PWEM [25], the dispersion curves do degenerate into the frequency of the single PCW in the symmetric DC made of a PCS at the degenerate or decoupling point in which $g(ka) = 0$. In addition, the eigenmodes switch at this degenerate point, i.e. the parity of the low-frequency dispersion curve is switched from odd to even, shown as figure 4(a). The energy remains in the same PCW when one sets the operation frequency at the decoupling point, but it does completely transfer into the other PCW after propagating a coupling length ($L = \pi/\Delta k$) on operating at a frequency departing from the decoupling point, where Δk is the wave vector mismatch of two modes at the operation frequency. On the other hand, for an asymmetric DC, the dispersion curves will not cross, but the eigenmodes do switch at the decoupling point at which the frequency difference is the smallest, as shown in figure 4(b). The eigenmodes localize mainly in one branch of the couplers as the operation frequency is set very close to the decoupling point that makes the lowest energy transfer around the decoupling point.

On increasing the height of the slab, the dispersion curves of the DCs or PCWs shift towards lower frequencies with the same wave vectors of the crossing point due to the similar electric field distribution of point defects as shown in figure 5(a). In the 2D PC whose height is infinite, the frequencies or dispersion curves are lower than those in the slab because the fields that spread into the air-cladding layers would lead to higher frequencies compared with the 2D PC [26]. Therefore, when one wants to design a decoupling point in a coupler made of PCS, one can do it using a 2D simulation. The dispersion curves will just shift towards higher frequencies when reducing the height of the PCS.

For designing multiplexing/demultiplexing, a PCS made of a triangular lattice is a better choice because the dispersion curves should cross in this structure that provides infinite coupling length at the designed decoupling point (frequency) and a finite coupling length at the other operation frequency departing from the decoupling point. The decoupling point can also be moved by varying the radius of the dielectric defect rods, as shown in figure 5(b). On reducing the radius of the dielectric-defect rods, the electric field will be less localized in the defects, which makes $|2\beta/\alpha|$ in equation (14) larger so that the decoupling point moves towards the lower wave vector. However, for a compact optical chip, square-lattice PCS is a better choice because there is no crossing point in this structure, as shown in figure 5(c). When a crossing point exists in the dispersion curves of the DC, the lower dispersion curve will bend down at a high wave vector. This makes the choice of a frequency, with only one propagation wave vector in each dispersion curve to realize a short coupling length, more difficult.

On the other hand, we consider an air-hole slab made of a triangular lattice with the dielectric constant, height of the slab and radius of the perfect holes being 12, 0.55a and 0.3a, respectively. Here, we use only the symmetric DC as a demonstration because a similar concept can be applied for the asymmetric air-hole DC. When the radius of air holes in a single PCW or DC is enlarged, the dispersion curve of the single PCW does not locate exactly between those of the DC particularly at a low wave vector, as shown in figure 6. Because a large band gap exists in the triangular lattice rather than in the square lattice, here we consider only an air-hole PCS with a triangular lattice in which the dispersion curves of the DC are always crossing. On enlarging the radius of the defect holes, as shown in figure 6(a), the electric field becomes less localized in the defects, which leads to an increased coupling coefficient P_1, a faster group velocity of the PCW and DC, and a shorter coupling length.

Figure 6(b) shows that the dispersion curves of DCs have a blue shift relative to the 2D case on decreasing the height

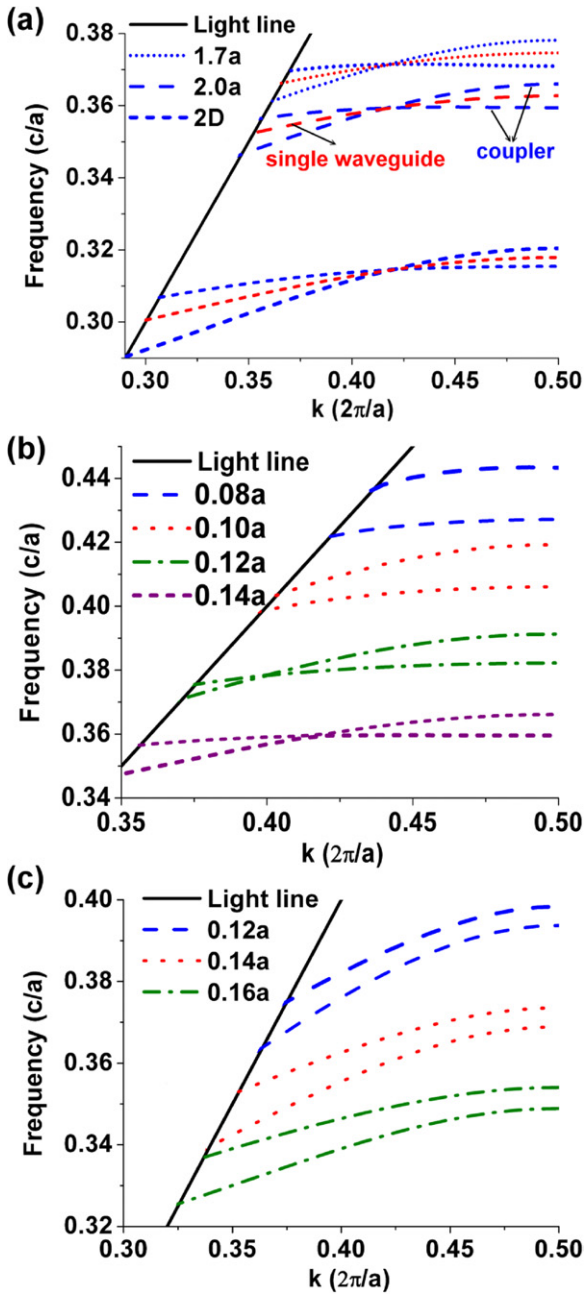

Figure 5. Dispersion relation curves of DCs or single PCWs in (*a*), (*b*) triangular lattices and (*c*) square lattices. The dielectric constant and radius of perfect dielectric rods are 12 and 0.2*a* with (*a*) radius of defect rods (r_d) being 0.14*a*; the height of the slab being 1.7*a*, 2.0*a* and infinite for 2D case; (*b*) the height of the slab being 2*a* and r_d being 0.08–0.14*a*; (*c*) the height of the slab being 2*a* and r_d being 0.12–0.16*a*.

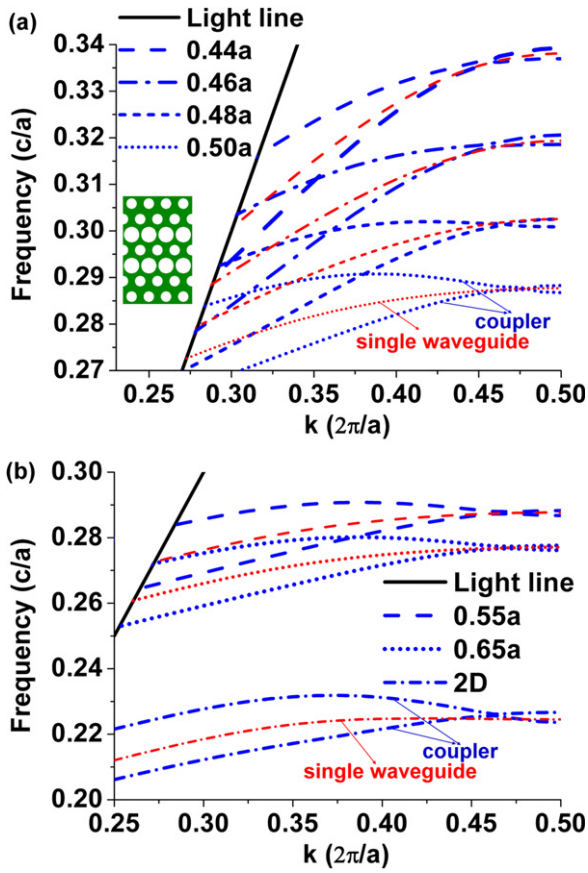

Figure 6. Dispersion relation curves of DCs or single PCWs in triangular lattices. The dielectric constant of the slab and radius of perfect holes are 12 and 0.3*a* with (*a*) the height of the slab being 0.55*a* and radii of defect holes (r_d) being 0.44–0.50*a*; (*b*) radius of defect holes (r_d) being 0.5*a* and slab height being 0.55*a*, 0.65*a* and infinite for the 2D case. The inset in (*a*) is the cross section of the LDC.

of the slab because the fields have spread into the air-cladding layers. However, they are no longer parallel to the dispersion curves of the 2D coupler. The group velocity of a single 2D PCW even becomes negative at a high wave vector, which is not observed in the dielectric-rod PCW because the signs of coupling coefficients P_2' are different in these two cases. Therefore, an intensive 3D simulation is necessary in designing an air-defect coupler made of an air-hole PCS.

Although the dielectric-rod PCS is more difficult to fabricate compared with an air-hole PCS and the air-hole DC made by enlarging the radius of holes to support single mode propagation faces significant scattering due to the disorder of air holes as compared with the PCW made by removing the air holes, the air-defect DCs possess a short coupling length which is ∼5*a* for an air-hole PCS and ∼10*a* for a dielectric-rod PCS. It is much shorter than that for the DC made of dielectric defects. Moreover, two eigenmodes exist in a single dielectric point defect. Based on the TBT, there would be two dispersion curves in a single PCW due to the coupling of these two point-defect eigenmodes. Therefore, there could be four dispersion curves existing in the photonic band gap of the PCS. The analyses become quite complex and it is not easy to get a simple design concept in dielectric defects. As one can reduce the manufacture disorder of air holes or dielectric rods by making an air-defect DC, the air-defect DC will be a better choice than the dielectric-defect DC.

6. Conclusion

We successfully used the TBT to derive the coupled equations to describe the physical properties of an optical coupler and PCW made of air-hole and dielectric-rod slabs. From these derived coupled equations, we found although the dispersion

curves can cross in symmetric couplers but never cross in asymmetric couplers, the eigenmodes switch at the decoupling point for both cases.

In dielectric-rod DCs, the coupling coefficients are dominated mainly by the electric field parallel to the rods. The field distributions of a point defect in the PCS and in the 2D PC are almost the same but the former has a higher eigenfrequency. Therefore, the dispersion curves of the coupler in the PCS will be nearly parallel to that in a 2D PC only with a blue shift in its frequency. In triangular lattices, the dispersion curves of the DC are crossed and the crossing point can be tuned towards a low vector by reducing the radius of the defect rods. For a square lattice, the dispersion curves of a DC hardly cross, which makes it easier to design a DC with a finite coupling length.

In the air-hole PCS, we found that the dispersion curve of the single PCW is no longer located at the centre of the curves of the DC and the group velocity may become negative. The dispersion curves in the slab are not parallel to those in the 2D structures. Therefore, a 3D simulation is necessary for designing air-defect waveguides. From the simulation results, the coupling length of this DC is approximately 5 lattice constants, which is much smaller than that made by removing the air holes.

Acknowledgments

The authors would like to thank the National Science Council of the Republic of China for partial financial support under grants NSC099-2811-M-006-028, NSC99-2112-M-006-017-MY3, NSC99-2221-E-009-095-MY3 and NSC 99-2112-M-034-002-MY3.

References

[1] Joannopoulos J D *et al* 2008 *Photonic Crystals: Molding the Flow of Light* (Princeton, NJ: Princeton University Press)
[2] Johnson S G *et al* 1999 *Phys. Rev.* B **60** 5751–8
[3] Johnson S G *et al* 2000 *Phys. Rev.* B **62** 8212–22
[4] Benisty H *et al* 1999 *J. Lightwave Technol.* **17** 2063–77
[5] Lin S Y *et al* 2000 *Opt. Lett.* **25** 1297–9
[6] Tokushima M, Yamada H and Arakawa Y 2004 *Appl. Phys. Lett.* **84** 4298–300
[7] Asakawa K *et al* 2006 *New J. Phys.* **8** 208
[8] Almeida V R *et al* 2004 *Nature* **431** 1081–4
[9] Momeni B *et al* 2009 *J. Nanophoton.* **3** 031001
[10] Yamamoto N, Ogawa T and Komori K 2006 *Opt. Express* **14** 1223–9
[11] Beggs D M *et al* 2008 *Opt. Lett.* **33** 147–9
[12] Notomi M *et al* 2004 *Opt. Express* **12** 1551–61
[13] Tanaka Y *et al* 2005 *IEEE J. Quantum Electron.* **41** 76–84
[14] Qu Y, Ren H L and Jiang C 2007 *IEEE J. Quantum Electron.* **43** 974–81
[15] Chien F S S *et al* 2007 *Phys. Rev.* B **75** 125113
[16] Huang C H, Hsieh W F and Cheng S C 2009 *J. Opt. Soc. Am.* B **26** 203–9
[17] Qiu M 2002 *Appl. Phys. Lett.* **81** 1163–5
[18] Zhou W D, Qiang Z X and Chen L 2007 *J. Phys. D: Appl. Phys.* **40** 2615–23
[19] Bayindir M, Temelkuran B and Ozbay E 2000 *Phys. Rev. Lett.* **84** 2140–3
[20] Mookherjea S 2005 *Opt. Lett.* **30** 2406–8
[21] Christodoulides D N and Efremidis N K 2002 *Opt. Lett.* **27** 568–70
[22] Huang C H, Hsieh W F and Cheng S C 2008 *J. Korean Phys. Soc.* **53** 1246–50
[23] Huang C H *et al* 2009 *Opt. Express* **17** 1299–307
[24] Huang C H, Hsieh W F and Cheng S C 2009 *J. Opt. A: Pure Appl. Opt.* **11** 015103
[25] Johnson S G and Joannopoulos J D 2001 *Opt. Express* **8** 173–90
[26] Zhang H *et al* 2006 *J. Opt. A: Pure Appl. Opt.* **8** 483–8